

See discussions, stats, and author profiles for this publication at: <https://www.researchgate.net/publication/370998033>

# Supersonic Nozzle Design for Arc Plasma Wind Tunnels

Preprint · May 2023

CITATIONS

0

4 authors, including:



**Oshri Ifergan**

Technion - Israel Institute of Technology

6 PUBLICATIONS 2 CITATIONS

[SEE PROFILE](#)



**David Greenblatt**

Technion - Israel Institute of Technology

185 PUBLICATIONS 4,659 CITATIONS

[SEE PROFILE](#)

Some of the authors of this publication are also working on these related projects:



Vertical Axis Wind Turbine Active Flow Control [View project](#)



Tethered Body Stabilization using Active Flow Control [View project](#)

# Supersonic Nozzle Design for Arc Plasma Wind Tunnels

Nir Bratman<sup>1</sup>

Rafael Advanced Defense Systems, POB 2250, Haifa, 3102102 Israel

Oshri Ifergan<sup>2</sup>

CoreFlow, Daliyat al-Carmel, 3005600, Israel

Moshe Berreby<sup>3</sup>

*IARD Sensing Solutions Ltd., Kibbutz Yagur, Israel*

David Greenblatt<sup>4</sup>

Technion – Israel Institute of Technology, Haifa, 3200003

---

<sup>1</sup> Senior Scientist.

<sup>2</sup> Chief Technical Officer.

<sup>3</sup> Modelling Group Senior Scientist.

<sup>4</sup> Professor, Faculty of Mechanical Engineering, AIAA Associate Fellow. davidg@technion.ac.il.

## **Abstract**

A Mach 4 parallel flow supersonic nozzle, intended for arc-plasma wind tunnel applications, was designed for high-pressure and high-enthalpy working point conditions. The objective was to ensure effective cooling and structural integrity under conditions of no shock wave formation and parallel flow streamlines at the nozzle exit. The design was performed using a simplified approach, enabling the rapid examination of feasible design parameters, which were subsequently validated against Reynolds-Averaged Navier Stokes computational methods and finite-element structural simulations. The simplified approach was subdivided into the aerodynamic design, using the method of characteristics; aerodynamic-heating predictions, using integral and reference temperature methods; nozzle cooling-jacket performance predictions, based on semi-empirical correlations; and structural considerations, based on the pressure-induced and thermally-induced stresses in a circular cylinder. The simplified approach showed excellent agreement with computational methods and simulations. In particular, local cooling water temperature differences in the high heat-flux throat region never differed by more than 0.2°C. Moreover, small inner and outer nozzle wall temperature overpredictions, that resulted from neglecting axial conduction, validated our conservative design approach.

## **1. Introduction**

In the field of aerothermodynamics, hot wind tunnels are an essential and efficient tool for the design of hypersonic vehicles, where the Mach number is matched to the desired flight conditions [1]. Arc plasma wind tunnels are particularly useful for studying the effects associated with re-entry and high-velocity vehicles. These are related to the very high aerodynamic heating encountered during hypersonic flight and the effectiveness of Thermal Protection Systems (TPS) [2]. Arc plasma wind tunnels can also simulate target thermal loading conditions without necessarily matching the Mach number. The aerothermodynamic design of supersonic and hypersonic nozzles require special attention, both in terms of the flow quality and in terms of effective cooling.

This paper presents a design methodology for supersonic nozzles used in arc plasma wind tunnels. The methodology is general, but the specific example presented here relates to the specifications of the high-enthalpy Technion Arc Plasma Tunnel (TAPT) [3]. The most common approach to supersonic nozzle design is to use computation fluid dynamics (CFD) which is time consuming. Additionally, effective cooling must be implemented in order to dissipate the high thermal loads imposed on the nozzle wall. In recent years, efforts have been made to account for chemical property variations and ro-vibrational relaxation states of molecules, at high temperatures by combining CFD and the method of characteristics (MoC) calculations [4] [5].

The objective of this work is to develop a rapid and simplified design methodology for arc plasma supersonic nozzles and to validate it against computational tools. An example is presented for the TAPT at design Mach numbers in the range of 3.5 to 3.9, which is suitable for two significantly different enthalpy conditions, under the facility constraints. The design must fulfil two main requirements. First, the aerodynamic design must ensure ideally expanded parallel flow at the nozzle exit section for both cases. Second, the nozzle wall temperature must be effectively cooled in order to remain below the maximum allowable wall temperature. Furthermore, thermal gradients must be minimized to eliminate the possibility of failure due to induced thermo-mechanical stresses.

## **2. Nozzle Parametric Design**

The nozzle parametric design is based on the 5 MW TAPT operating conditions described in [6]. The nozzle is intended to work at vacuum conditions in order to attain the target Mach

numbers. To this end, the facility is equipped with a vacuum chamber, evacuated via a two-stage steam ejector, with a background pressure of 25 mbar at 250 g/s. Two different working point conditions were selected, namely a 2 MJ/Kg “high-pressure” working point (case 1); and a 7 MJ/Kg “high-temperature” working point (case 2). The details of each working point are given in Table 1). Aerodynamic heating conditions were simulated according to the gas total specific enthalpy and mass flowrate through the choked nozzle, in conjunction with a semi-empirical relation, based on dimensional analysis and gas dynamics theory, described in [7]. Both cases were constrained by throat and design nozzle exit diameters of 25 and 94 mm, respectively. A design performance map was generated by assuming a calorically perfect gas with heat capacity ratios  $\gamma$  of 1.2 and 1.3, which are the typical values at these enthalpies, in order to obtain a closed-form analytical solution. We will show below in section 4, that this assumption is valid for preliminary estimates.

**Table 1. Two operating point conditions calculated under the calorically perfect gas assumption.**

|   | Case 1: high-pressure | Case 2: high-temperature |
|---|-----------------------|--------------------------|
| Air mass flow rate (g/s)                  | 243                   | 112                      |
| Specific total enthalpy (MJ/kg)           | 1.75                  | 6.70                     |
| Total temperature (K)                     | 1,800                 | 4,000                    |
| Total pressure (bar)                      | 5.33                  | 3.90                     |
| Mach number at the nozzle exit            | 3.90                  | 3.52                     |
| Nozzle exit static temperature (K)        | 478                   | 1785                     |
| Approximate heat capacity ratio, $\gamma$ | 1.3                   | 1.2                      |
| Exit diameter (mm)                        |                       | 94                       |
| Throat diameter (mm)                      |                       | 25                       |

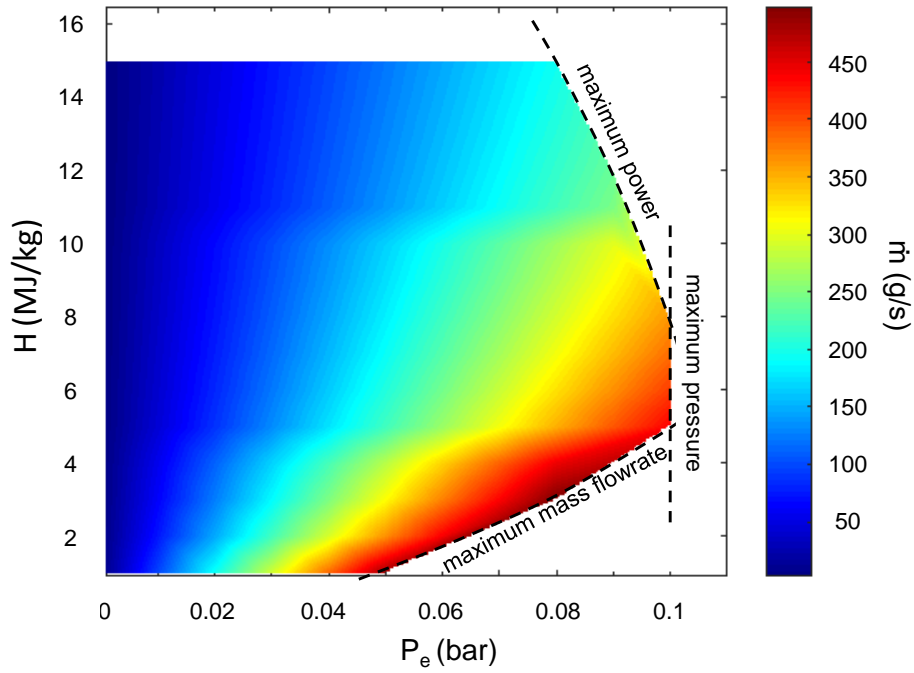


**Figure 1. Nozzle performance map based on the TAPT operating conditions and the two-stage ejector performance.**

Figure 1 shows the performance map of the selected adapted nozzle, under the facility constraints. The map is bounded on the top, right and bottom by the tunnel maximum electrical power, maximum plenum pressure, and maximum mass flowrate, respectively. The three gradients seen in the mass flow are due to different gas heat capacity ratios assumed for the different enthalpies according to values of air in chemical equilibrium at constant pressure versus temperature [8].

### 3. Aerodynamic Design

Having set the nozzle parameters, the method of characteristic (MoC) [9] was used to design the contour for uniform and parallel flow without shocks for both cases. The input parameters are Mach number ( $M$ ), pressure ( $P_e$ ) and temperature ( $T_e$ ) at the nozzle exit, the gas heat capacity ratio ( $\gamma$ ), and the throat diameter ( $D^*$ ), respectively. The outputs are the nozzle contour and the flow properties at each cross-section, based on isentropic relations [9]. The geometry was corrected using the standard flat plate displacement thickness relation, which is conservative, due to the favorable pressure gradients [9]. Design contour estimations were

based on Case 1 conditions (highest pressure/low enthalpy), since it requires a longer nozzle allowing the flow to expand and accelerate more gradually. This was considered to be valid for lower pressure (higher enthalpy) case as well, because higher acceleration is less likely to produce flow separation. The conservative boundary layer displacement thickness correction produced small reductions in diameters, namely 1.5% and 3.5% for Cases 1 and 2, respectively. The wall geometry was smoothed using the ratio of 5<sup>th</sup> and 4<sup>th</sup> order polynomials, with a correlation coefficient  $R^2 = 0.9999$ .

To verify the resulting nozzle contour, a RANS code [11] was employed with the  $k-\omega$  SST turbulence model [12], assuming a constant specific heat ratio and isentropic flow (see Figure 2). The code employs a finite-volume method and has second-order accuracy in space and time [13]. In addition, the solver is capable of simulating flows of thermally-perfect, multicomponent gas mixtures in chemical equilibrium or non-equilibrium. The equations were solve using an axi-symmetric coordinate system with 299 streamwise points and 150 radial points. The grid density increased in the region of the nozzle and in the vicinity of the wall such that the  $y^+$  values of surface-neighboring cells were less than 0.5 for all simulations.

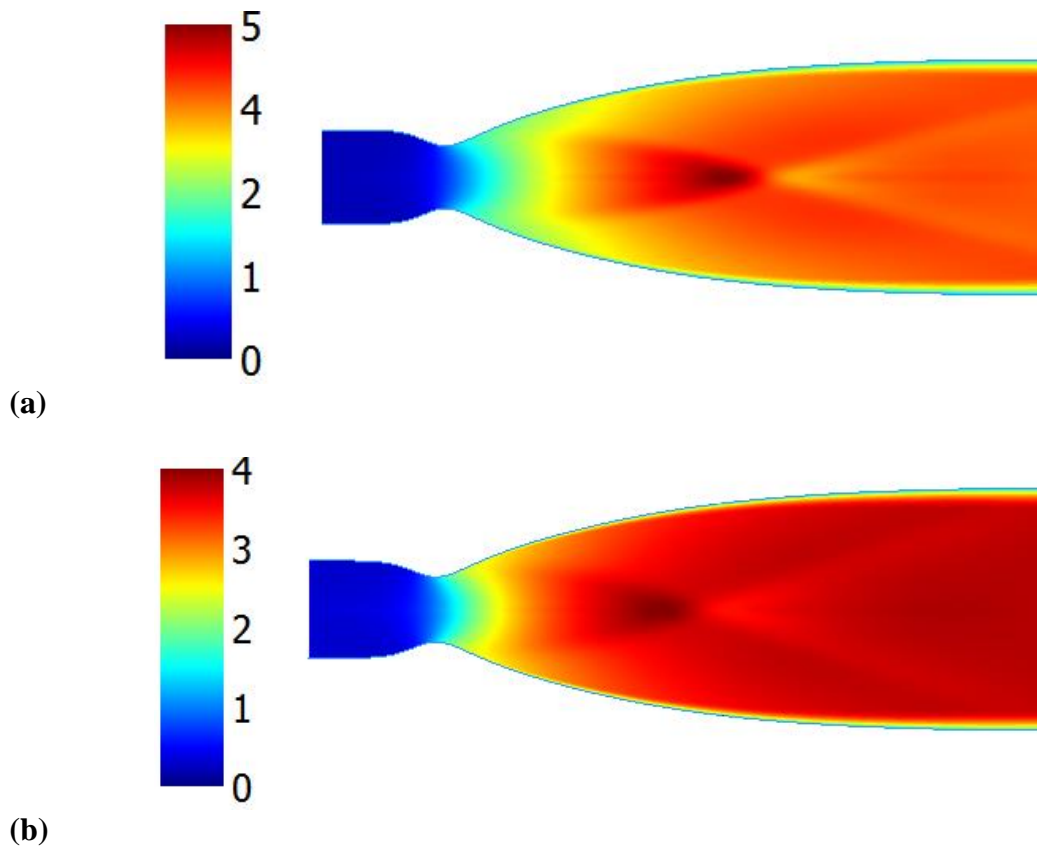


**Figure 2. Mach number distributions in the nozzle from CFD based conditions of chemical equilibrium, for (a) the high-pressure working point; and (b) the high-temperature working point. Note the different legend scales.**

In the high-pressure case, the nozzle could have been designed with a slightly longer expansion region (not shown), which is longer than the minimum length required for the high-temperature case. The reason for the different lengths is the fact that the specific heat ratio was assumed as constant while it, in fact, increases from a value of 1.3 to 1.4 as the temperature drops with the flow expansion. Despite the non-optimal shape, the CFD results indicate that the results are indeed sufficient as the flow properties are still uniform and parallel at the exit (flow angle relative to the wall is within  $1.4^\circ$  variations in both cases). Using the boundary layer relation for a turbulent flat plate, the boundary layer [10] correction gives the same order of magnitude given by the CFD analysis.

#### **4. Aerodynamic Heating**

For high Mach number supersonic nozzles employed in conjunction with a high enthalpy wind tunnels, accurate estimates of the heat transfer are critical. Four different methods were evaluated, namely the Bartz method [18][19], two forms of the reference temperature method [20][21], and the modified momentum energy integral method (MEI) [22][23]. The reference temperature methods employ the classical Dittus and Boelter [23][20] correlation. The relative strengths of these methods are evaluated by comparing them to the computational results. Only forced-convection heat transfer from the high enthalpy flow to the wall was considered, because radiation heat transfer from the hot air, which is a transparent gas with very low emissivity, is negligible [14][16]. Fluid properties along the nozzle were calculated using the isentropic relations, with a constant heat capacity ratio for each case, assuming chemical equilibrium. The equilibrium thermal properties (Prandtl number, viscosity, specific heat, and characteristic velocity) were obtained using NASA CEA (Chemical Equilibrium Applications) program described in [17]. Additional computations were performed for the high-temperature condition case, where both frozen chemistry and finite-rate chemical kinetics were modeled using the 5-species, 11-reactions Dunn and Kang reaction set [24].

An in-house code was developed to calculate the nozzle heat transfer properties, based on the NASA procedures and correlations for throat heat transfer in rocket nozzles [20][32][22]. The program solves the two integral momentum and energy equations by an implicit finite difference scheme while calculating the local shape factor, recovery factor, Stanton number, and friction coefficient using well-known correlations. The wall, which is much colder than the nozzle airflow, might cause the airflow concentrations to change adjacent to it. It is thus

reasonable to assume that no recombination occurs at airflow temperature lower than approximately 2,500 K. Indeed, oxygen molecule dissociations begin around this temperature under atmospheric pressure, and even at higher temperature for higher pressure. The heat transfer coefficient expression for the surface heat flux was defined in terms of recovery enthalpy.

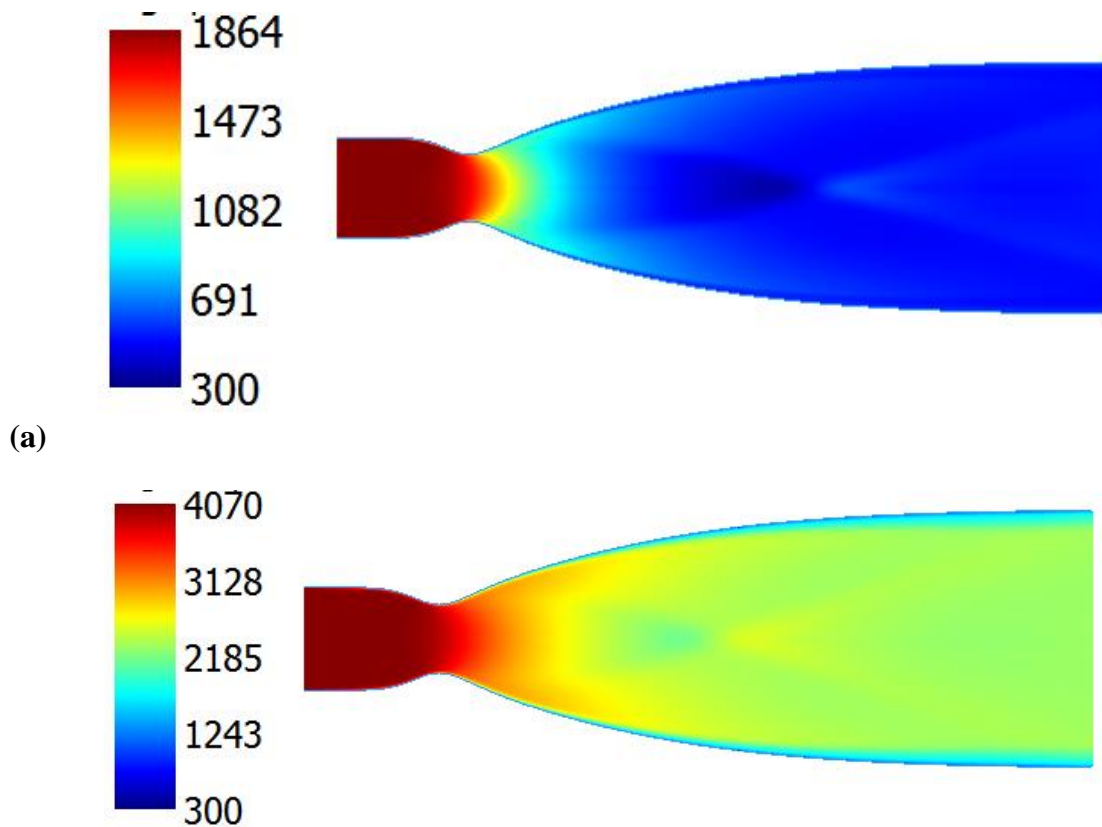
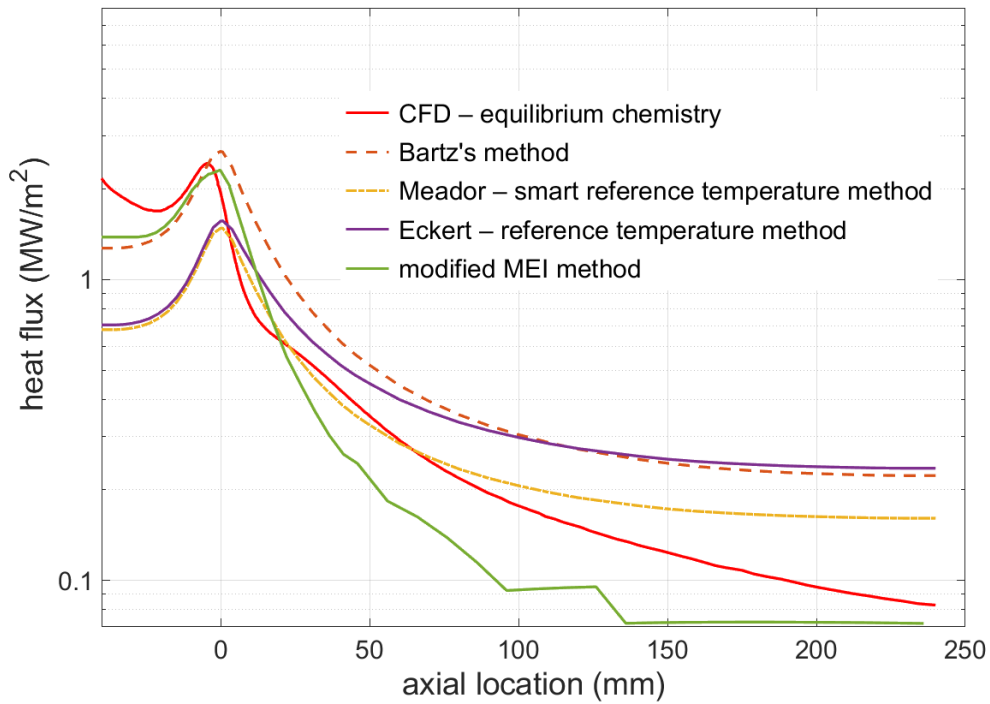
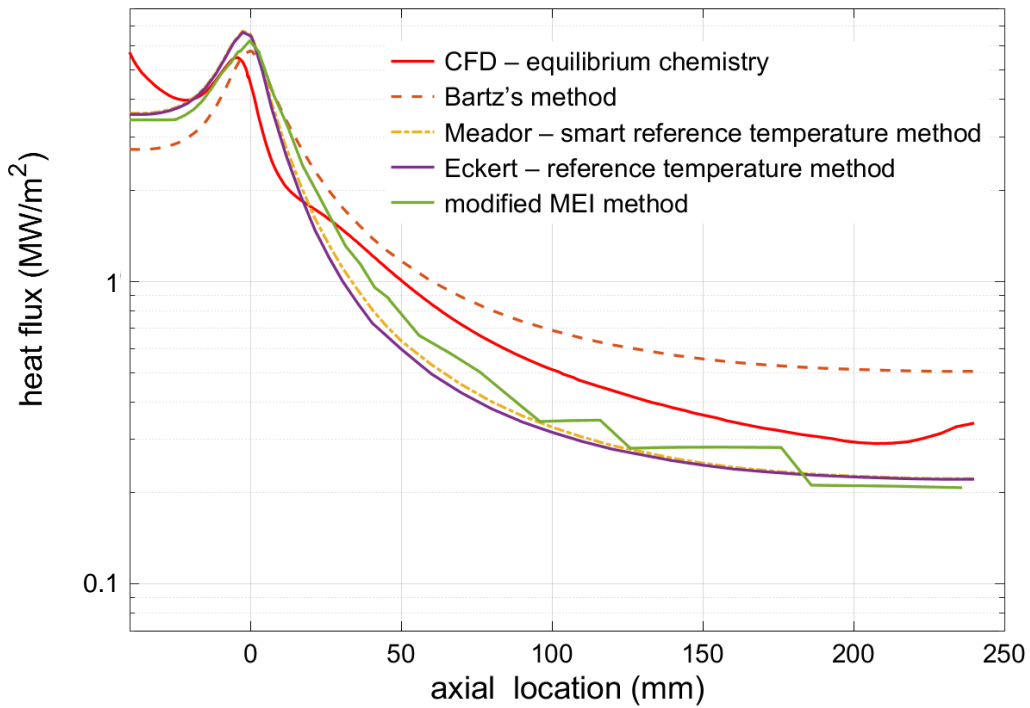


**Figure 3. Temperature distributions in the nozzle from CFD based on chemical equilibrium, for (a) the high-pressure working point; (b) the high-temperature working point. Note the different legend scales.**

The CFD code solves the entire flow field and accounts for energy losses to the cold wall, unlike isentropic flow assumed in simplified calculations, and chemical reactions taking place in the nozzle. The surface in the CFD analysis is modeled as a 300 K isothermally cold wall, which is conservative for the expected heat flux. This model was adopted for comparison and validation only, because in practice wall temperatures are much higher and vary along the nozzle (see Figure 3). An adiabatic wall analysis was also performed for both cases in order to determine the recovery temperature and compare it to the simplified calculated values.



(a)



(b)

**Figure 4. Wall heat flux comparisons between simplified analyses and computational results based on chemical equilibrium, for (a) the high-pressure working point; (b) the high-temperature working point.**

Heat flux results for the simplified analyses are compared to the computational results in Figure 4. At the entrance to the nozzle, no boundary layer boundary layer thickness boundary condition was imposed and this resulted in unrealistically high local heat flux (cf. [19]). Nevertheless, the heat flux peak is displaced slightly upstream of the throat due to viscous effects. For both cases, Bartz's method and the modified MEI method produce the greatest accuracy at the throat in absolute terms. Both reference temperature methods underpredict throat heat transfer for the high-pressure case and overpredict throat heat transfer for the high-temperature case. The computed heat flux drops sharply downstream of the throat, which is over-predicted using Bartz's method and is also consistent with results shown in refs. [19][24][27][25]. This finding is consistent with other investigations [22][19][20], that show over-predictions of up to 50% downstream of the throat. The modified MEI method [20][22] attains a far greater accuracy immediately downstream of the throat, but then underpredicts the heat transfer for  $x > 25$  mm. The reference temperature methods generally overpredict and underpredict the downstream heat transfer for the high-pressure and high-temperature cases, respectively.

Computations with frozen chemistry and finite-rate chemical kinetics are compared to that with chemical equilibrium in Figure 5. The comparison show that the flow remains effectively in equilibrium up to the throat and then transitions to a frozen state, as the Mach number increases. Since the reactive flow is found to be mostly frozen, the absence of chemical reactions causes the temperature to be lower. This results in lower heat loads on the nozzle wall than in equilibrium flow. Finite-rate analysis shows close results with frozen conditions toward exit plane of the nozzle since the diverging section is mostly frozen. The maximum heat load on the other hand, as seen in Figure 5, was found to be much closer to that of the equilibrium case since these conditions exist up to the throat. To ensure that finite-rate results did not under-predict the physical phenomena due to catalytic surface effects of the wall, another simulation was conducted where the wall was defined as super-catalytic. The near-wall concentration change due to recombination, was determined according to the wall temperature to produce conservative results. As can be seen in Figure 5 the results are indeed higher, reaching the same peak value as in the equilibrium analysis and then decreasing as the flow becomes frozen in the divergence section.

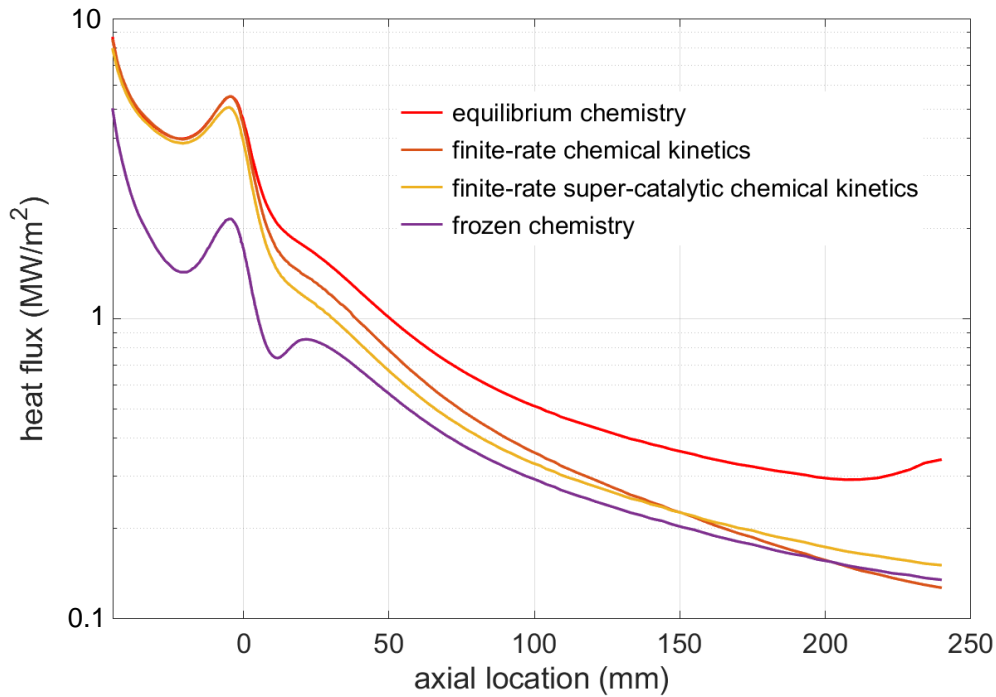


**Figure 5. Wall heat flux computations for the high-temperature working point based on different gas reaction assumptions.**

The equilibrium hypothesis, while potentially overestimating the chemical kinetics and the heat load, was found to yield very good results, allowing a less resource-consuming analysis. In the high-pressure case, negligible differences exist while in the high-temperature case the differences are relatively small. Thus, these results validate the use of the conservative equilibrium flow assumption for the nozzle design.

## 5. Structural Analysis

A major consideration in the selection of the wall material, is its ability to operate at elevated temperatures with high strength and toughness. Copper was chosen as the nozzle material due to its excellent thermal characteristics and its ability to withstand harsh thermal and mechanical loads [28][29], as well as its compatibility with deionized cooling water. To determine the wall thickness, stresses induced by the diameter change in the axial direction are neglected. This corresponds to a two-dimensional axi-symmetric problem, equivalent to a hollow cylinder while accounting for the changes in diameter, pressure, and heat flux [30]. Copper mechanical properties at 573K for hard and pure copper were used [28][29]. Finally, nozzle structural analysis is performed to calculate the stresses induced by both internal and external pressures together with the thermal-induced stresses. All stresses are then summed, and the safety factor is calculated using four different well-known failure criteria for comparison, namely: maximum normal stress, maximum shear stress, maximum strain and octahedral shear stress criteria. The simplified design calculations are compared with a three-dimensional coupled thermal-structural simulation conducted using the commercial software Ansys©.

The analysis was performed relative to the throat section when the heat load is highest (see Figure 6). The analysis assumes the conservative external and internal pressures of 30-bar and 1-bar respectively. Since both heat load and induced pressure conditions are conservative, a relatively low safety factor for the thermal stresses can be used. We can see in Figure 7 that a thicker wall reduces the pressure-induced stress while increasing the thermally-induced stress. Summing the two, a stress optimum can be found, corresponding to a wall thickness of approximately 1 mm. The safety factors calculated using the four different criteria yielded virtually identical results (maximum normal criterion result is shown in Figure 7) allowing the relatively large range of wall thicknesses. For purposes of manufacturing convenience, a 3 mm wall thickness was selected, corresponding to a total circumferential stress of 130 MPa as indicated in Figure 6.

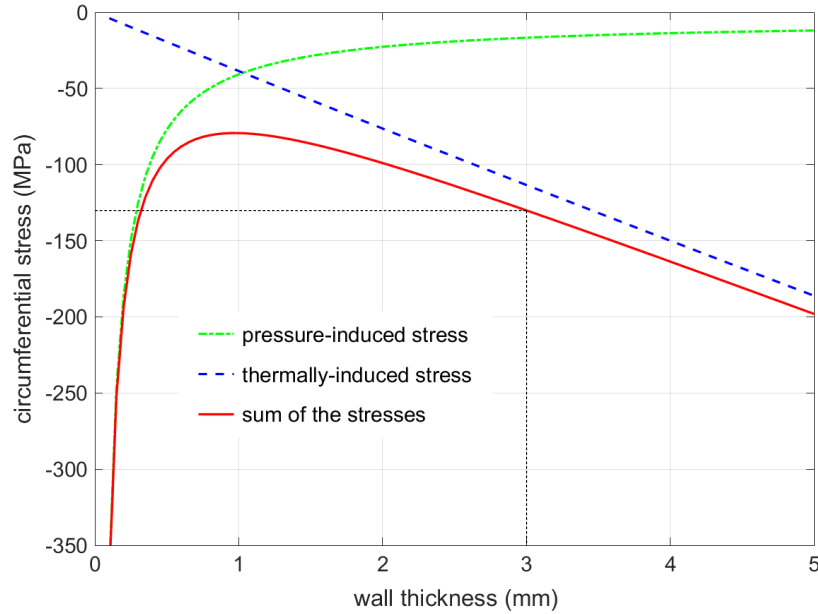


**Figure 6. The induced stresses for different wall thicknesses at the throat. Heat load = 8 MW/m<sup>2</sup>, internal pressure = 1 bar, external pressure = 30 bar.**

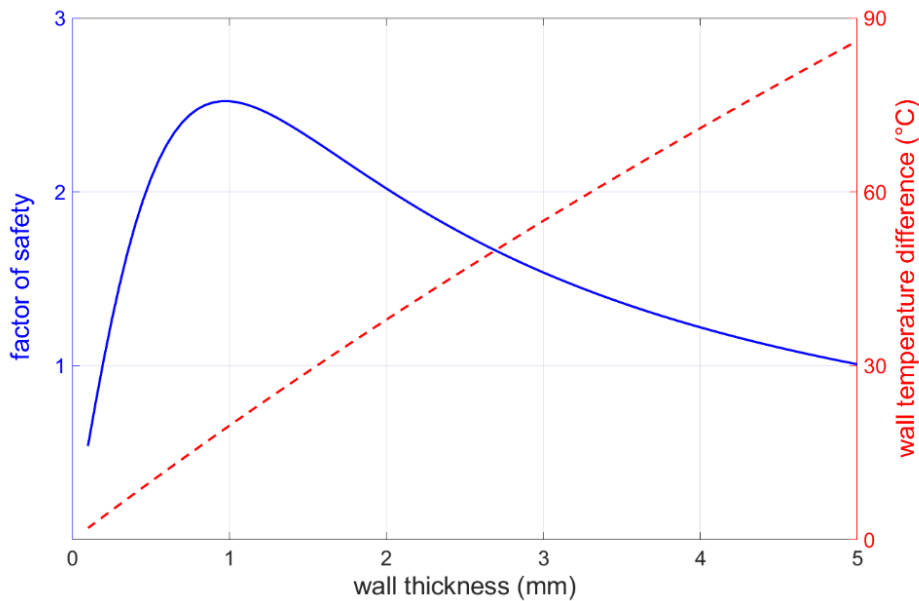
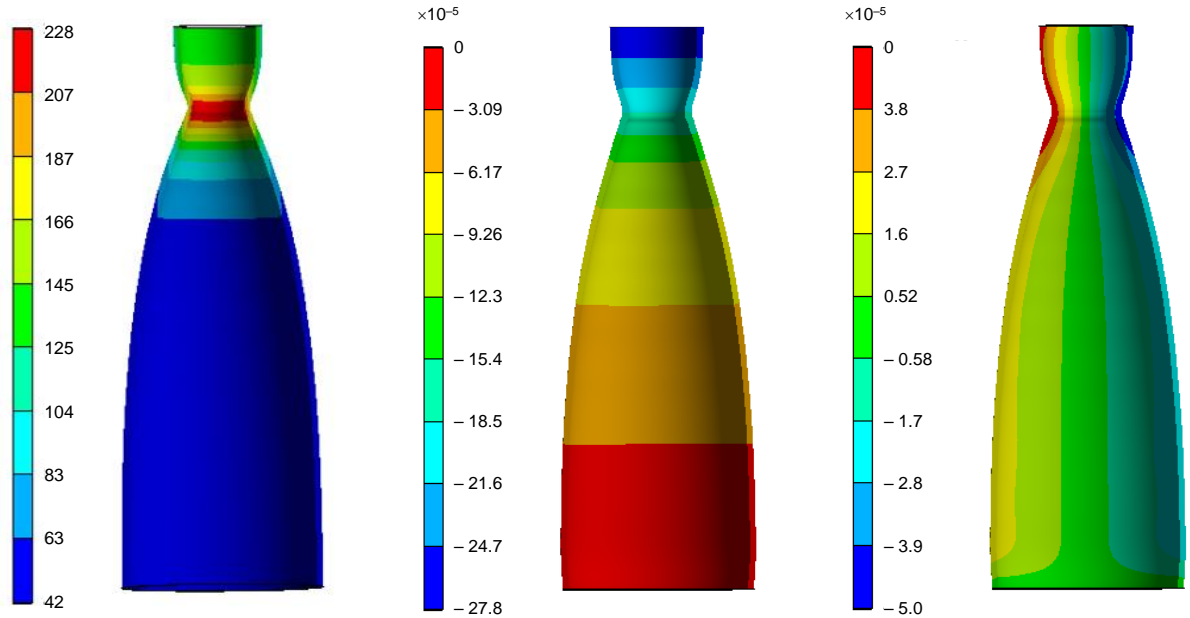


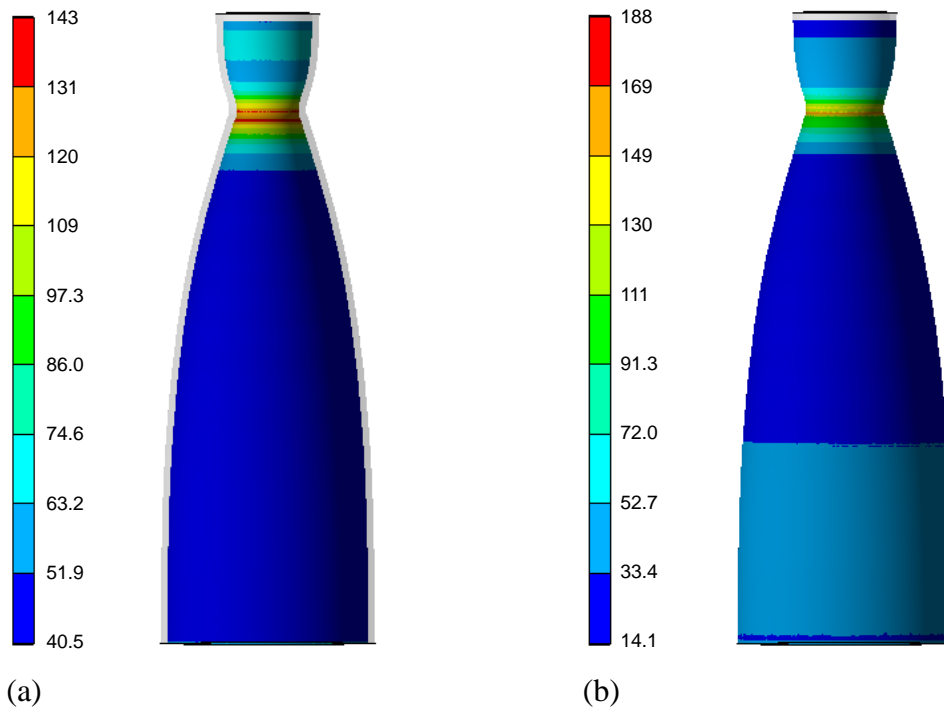
**Figure 7. Factor of safety for different wall thicknesses at the throat, corresponding to Figure 6. Heat load = 8 MW/m<sup>2</sup>, internal pressure = 1 bar, external pressure = 30 bar.**

The nozzle temperature and its expansion were calculated yielding a maximum temperature of 227°C at the throat section, and very small radial expansion and an expansion of 0.3 mm in the axial direction (Figure 8). Moreover the resulting maximum stress is comparable to that of the simplified analysis (130 MPa, indicated in Figure 6 versus 143 MPa shown in Figure 9a), based on a safety factor of 1.4. The safety factor is in fact even higher, because a conservative

heat load was assumed. Finally, it is important to ensure that the nozzle can expand in the axial direction, otherwise the stresses would dramatically grow above the failure point. This is physically realistic because, on the TAPT, the plenum section connected to the nozzle entrance is mounted on wheels and therefore it allows the nozzle to freely expand.



(a) temperature (°C)      (b) Axial deformation (m)      (c) radial deformation (m)  
**Figure 8. Nozzle temperature and directional deformations based on a three-dimensional coupled thermal-structural simulation conducted using Ansys©.**



(a)      (b)  
**Figure 9. The nozzle von-Mises equivalent stress variation in MPa, for (a) the internal wall; and (b) the external wall.**

## 6. Cooling System

### 6.1 The Cooling Design Configuration

The high heat load on nozzle walls requires a robust cooling design in order to prevent damage during a run at high enthalpy. The thermal model of the system can be described using the Newtonian resistor model as depicted in Figure 10. To this end, the heat balance, when simplified into a straight wall problem, can be written as:

$$q'' = h_a(T_r - T_{w,h}) = \frac{k}{\delta}(T_{w,h} - T_{w,c}) = h_c(T_{w,c} - T_c)$$

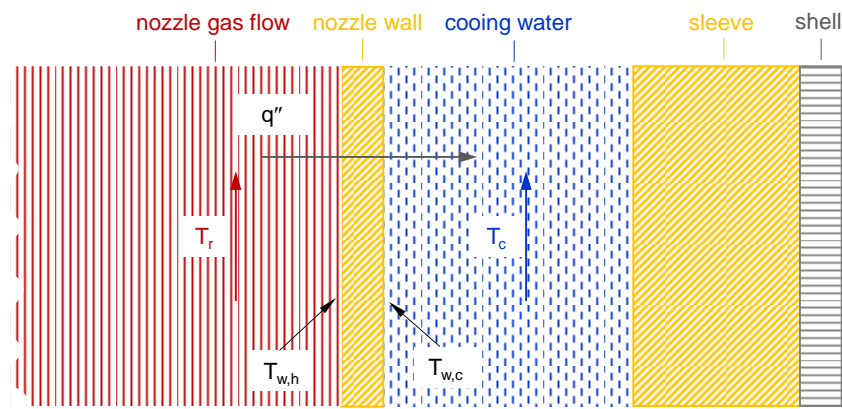


**Figure 10. Newtonian thermal resistor model schematic.**

Since the major cooling difficulty is located at the upstream nozzle contraction area and particularly at the throat, the cooling design concept was arranged so that the water would enter the cooling jacket at the contraction side section. The relatively low water temperature produces a greater heat transfer rate in the contraction region with an increased convection coefficient at the throat due to higher local velocities. The water temperature increases as it progresses along the annular extent of the outside nozzle wall.

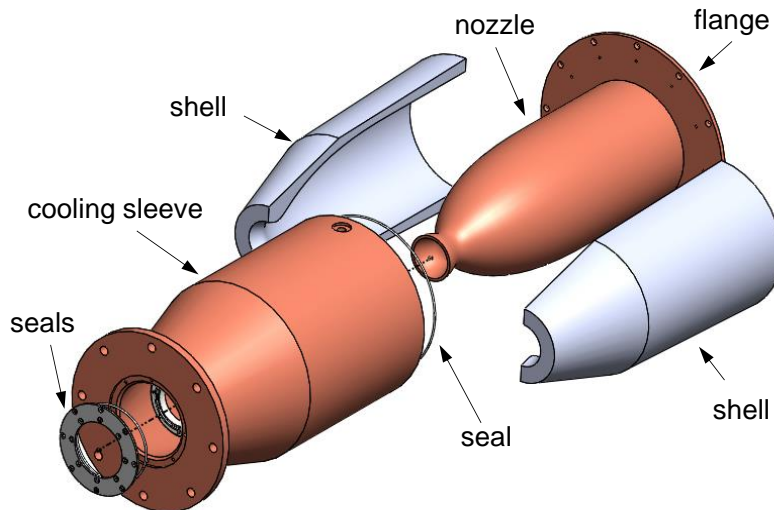


**Figure 11. Exploded view of the conceptual nozzle cooling assembly.**

The mechanical design concept comprises three main components shown in Figure 11, namely: the convergent-divergent nozzle, the cooling sleeve, and two half-shells. This configuration ensures conventional manufacturing processes. The copper nozzle and the sleeve are manufactured from copper using a conventional CNC manufacture process, while the two sleeves are made from any low weight material suitable for high-temperature, such as Vespel, which is either machined or printed. The shells are placed over the nozzle body and the sleeve locks the assembly. Seals are placed at the nozzle inlet and sleeve surfaces.

In the application, cooling is realized using deionized water to cool of the arc plasma tunnel, supplied by a 400HP centrifugal water pump from a 40m<sup>3</sup> reservoir available at the TAPT. It is supplied by a constant pressure of 35 bar, with a water mass flow of up to 125 kg/sec while 40 kg/sec is typically sufficient for the tunnel cooling sections. A 5-bar pressure drop results from losses between the inlet and outlet manifolds. The hydraulic resistance is given by the nozzle cooling sleeve and by the inlet and outlet tubes attached to the manifold. The existing tubes which are in current use in the facility are plastic tubes with a diameter of 10 mm and a length of up to 1.5 m.

## **6.2 Heat Transfer and Hydraulic-Loss Calculations**

The heat transfer coefficients and the wall temperature were calculated along the entire nozzle neglecting the heat spreading of the cooper (conservative) using an in-house code. It solves the coupled aerodynamic and concentric annulus cooling flow while taking into account the number of machined tunnels along the nozzle wall in different dimensions and corner angles.

After the parametric study, a more detailed finite elements 2D axisymmetric model is used to calculate the wall temperature by introducing the spreading effects.

The convection coefficients as a function of Nusselt number, based on the turbulent Dittus-Boelter equation, produces low estimates. Hence, four additional concentric annulus flow correlations were evaluated, namely the McAdams correlation (corrected Dittus-Boelter correlation); the Foust-Christian correlation; Davis's correlation; and the Petukhov-Roizen correlation. Modifications to the Nusselt number due to the surface roughness and wall curvature were considered, but ultimately not included due to their negligibly small effect. The hydrodynamic entry length, having the improved cooling effect, can be calculated by an empirical correlation taken from Yunus and Cimbalá [31]. Nevertheless, the flowfield was considered to be fully developed, which is a conservative approximation, since the cooling effects increase in the developing region.

The cooling water enters at ambient and temperature increases along the nozzle, while being continually heated by the nozzle wall. The heat flux depends on the wall temperature which is a function of both the external cooling and the internal aerodynamic heating. Therefore, an iterative convergence procedure was required to obtain the wall and the cooling water temperatures under steady-state conditions.

The cooling water total pressure drop was comprised of friction losses, expansion losses and contraction losses. The friction factor ( $f$ ) was calculated using the Moody diagram [33] and its equivalent Colebrook equation for turbulent flow at every location along the flow. Due to uncertainties in roughness height, experimental error, curve fitting of data, etc., the Colebrook equation is generally considered to have an accuracy of 15% over its entire range. Nevertheless, an approximate explicit relation for  $f$  proposed in [32] produced differences as small as 2% when compared to results of the Colebrook equation. The surface roughness ( $\epsilon$ ) was taken as 0.0015 mm, which the recommended value of copper and plastic for the nozzle cooling sleeve and the two connecting tubes [32]. The expansion and contraction coefficients  $k_e$  and  $k_c$  were obtained from the empirical Borda-Carnot equation presented in [33]. Friction, expansion and contraction losses were summed and employed in the standards modified mechanical energy (Bernoulli) equation.

## 7. Results and Computational Validation

In this section, the final configuration based on the simplified design procedure, is compared with computational results. The configuration has a cooling jacket with a 2 mm wide annular cooling channel, with a variable relative surface roughness of  $\varepsilon / D_h = 0.0015 / D_h$  and a minimum mass flowrate of 2.5 kg/s at 30°C. The results presented here are for the most extreme working point, namely the high-temperature case, and is based on the conservative MEI predictions previously presented (see Figure 4). The pressure drop calculation is based on a 30-bar system supply pressure, via 1.5m long piping with an internal diameter of 10 mm.

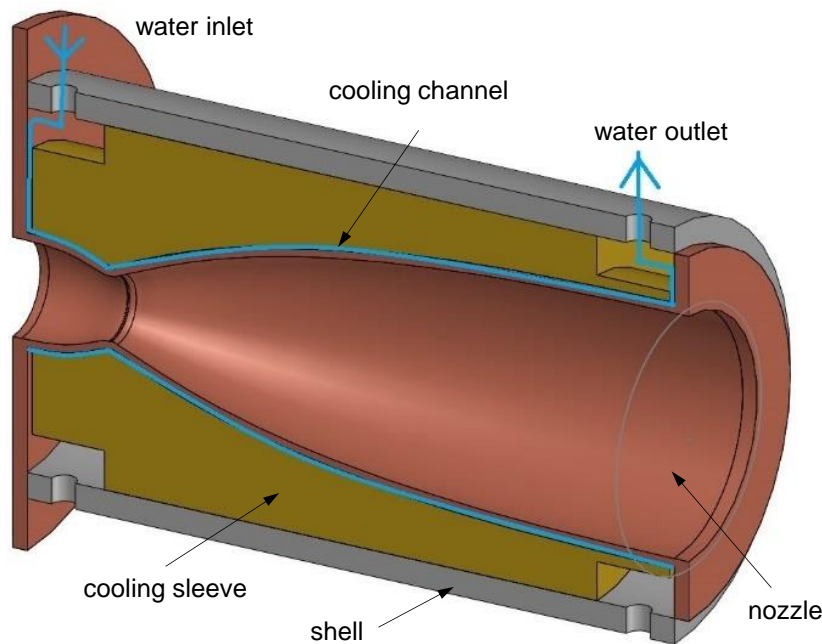


**Figure 12. Simplified three-dimensional CAD model is used for the nozzle cooling simulation.**

For the comparison, water cooling simulations were conducted using the commercially available Siemens NX Advanced Finite Element Simulation software©. The boundary conditions for the thermo-mechanical simulation were identical to those used in the design calculations. The simplified 3-D CAD model employed for the simulations has one water inlet and one water outlet as shown in Figure 12. The nozzle components, as well as the water, were meshed with 3D tetrahedral elements and an unstructured tetrahedral mesh was used in conjunction with wall functions. Two different turbulence models were used in order to verify the results, namely a  $k-\varepsilon$  model and the mixing-length model. For the  $k-\varepsilon$  model, wall functions were employed in order to avoid the additional computational cost associated with resolving

the viscous sublayer. For the mixing length model, the viscous sublayer was resolved using the van Driest near-wall modification and the outer (wake) region was independent of the wall coordinate. Despite the significant model differences, the water and wall temperature results never differed by more than 3%.

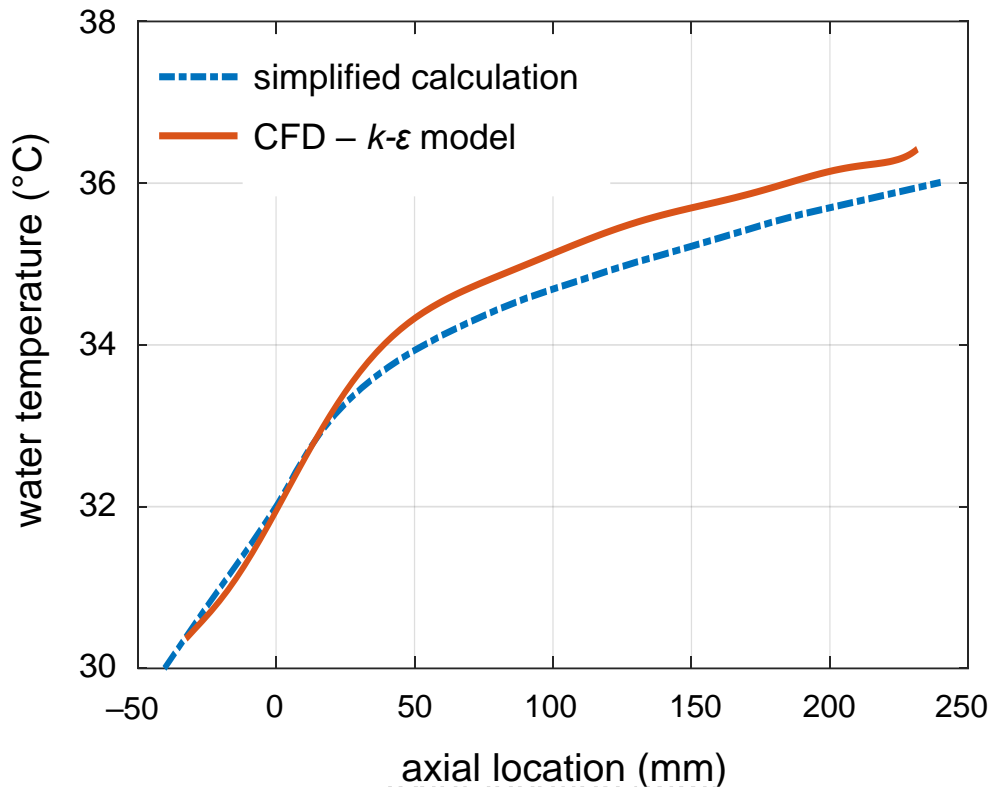


**Figure 13. Comparison of the cooling water temperature variation predicted by the simplified model and simulation.**

Cooling water and wall temperature comparisons are shown in Figure 13 and Figure 14, respectively. Immediately downstream of the water inlet, the cooling water increases sharply towards the nozzle throat due to the large heat flux in this region (Figure 13). This is shown by both the simulations and the simplified calculation, where the local temperatures never differ by more than 0.2°C. This close agreement is a particularly encouraging, because the heat flux (Figure 4b) and stresses (Figure 9) are highest at the throat. Downstream of the throat, the rate at which the temperature increases (or slope), reduces significantly with comparable results for both cases. Nevertheless, the simplified calculation underpredicts that of the simulation by as much as 0.5°C. The differences may be due to the large increases in the annual area, which by continuity can be shown to result in an adverse pressure gradient. This is not accounted for in the simplified model. In fact, the pressure drop across the nozzle is 10% smaller for the simplified calculation.

The inner and outer nozzle wall temperatures predicted by the simulations and simplified model (Figure 14), also show excellent agreement. The small model over-predictions upstream of the nozzle may be due to the localized cooling water inlet to the annular channel in the simulations versus the annular assumptions associated with the simplified model. However, the simulation peaks are lower and flatter, downstream of they exceed the model values. The reason for this is that the heat transfer conducts axially as well as well as radially in simulations, whereas the model does not account for this. Thus, the wall acts as a heat spreader which reduces the peak temperature predicted by the model, thereby resulting in a more uniform wall temperature. We therefore concluded that the local peak overprediction by the model is conservative and can be used with confidence for design calculations.

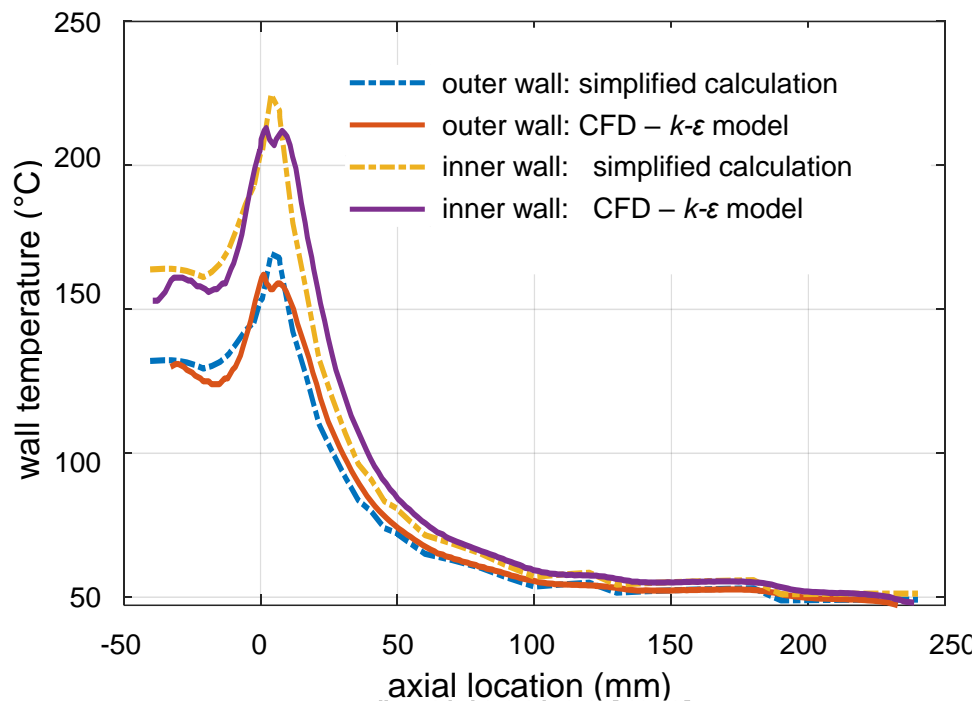


**Figure 14. Comparison of the inner and out wall temperature variations predicted by the simplified model and simulation.**

## 8. Conclusions & Future Research

A contoured Mach 4 supersonic nozzle for the Technion Arc Plasma Tunnel facility was designed based on a general methodology, that was established for future nozzle designs. The final nozzle configuration was 300 mm in length, with a 25 mm throat diameter and a 94 mm exit diameter. The nozzle was designed to withstand both high-pressure (5.33 bar, 1800°C) and high-temperature (3.90 bar, 4000°C) conditions, without exit shocks, and with parallel, uniform flow properties. A simplified design methodology was developed that included several in-house computer codes, in order to obtain rapid and accurate parameters with a choice of different methods. The aerodynamic design employed simplified calculations based on the method of characteristics and isentropic relations. The results were validated by CFD and indicated that the flow is in equilibrium upstream of the throat and becomes frozen as the Mach number increases. The best simplified methods used for predicting heat fluxes were the MEI and Bartz methods, with 12% and 9% errors, respectively, compared to CFD. Regarding nozzle cooling design, the Dittus-Boelter correlation was used as the most conservative and yielded results that were comparable to CFD.

An optimum wall thickness of 1 mm was estimated by analytical calculations, but a 3 mm wall thickness was selected due to manufacturing costs and found to be adequate mechanically. The simplified calculation showed a very good agreement with the results obtained by a finite element thermo-mechanical simulation. The simplified relations established between the different parameters facilitated rapid scaling approximations. Future research will be aimed at manufacturing the nozzle and validating its design by experiments. Several diagnostics may be implemented at the nozzle exit such as Schlieren visualization to validate the uniformity and deviations from parallel flow streamlines. Water temperature measurements at the inlet and outlet of the nozzle will be measured using axially and circumferentially-mounted temperature transducers to fully validate the fidelity of the simplified procedure.

## References

- [1] Bertin, J.J. “Hypersonic Aerothermodynamics,” AIAA Inc., Washington, DC, 1994, page 169. <https://doi.org/10.2514/4.470363>.
- [2] Marren, D.E. and Lu, F.K., “Advanced hypersonic test facilities,” Progress in Astronautics and Aeronautics, American Institute of Aeronautics and Astronautics, Vol. 198, 2002, pp. 375-402. <https://doi.org/10.2514/4.866678>.
- [3] Nabi, A, Barak, M. And Seginer, A., “Technion Arc Tunnel Calibration and Performance Prediction,” 70<sup>th</sup> Semi-annual Meeting of the Supersonic Tunnel Association, Lytham, Lancashire, UK, 11-12 October, 1988.
- [4] Chan, W.Y.K., Jacobs, P.A., Smart, M.K., Grieve, S., Craddock, C.S. and Doherty, L.J., “Aerodynamic Design of Nozzles with Uniform Outflow for Hypervelocity Ground-Test Facilities,” *AIAA Journal of Propulsion and Power*, Vol. 34, No. 6, 2018, pp. 1467-1478. <https://doi.org/10.2514/1.B36938>.
- [5] Starshak, W.C., Butler, C. and Laurence, S.J., “Method of Characteristics Design of High-Temperature Wind Tunnel Nozzles with Vibrational Relaxation,” AIAA Aviation Forum, 2018 Aerodynamic Measurement Technology and Ground Testing Conference, June 25-29, 2018, Atlanta, Georgia. <https://doi.org/10.2514/6.2018-3565>.
- [6] Ifergan, O, Berreby, M. and Greenblatt, D., “Simultaneous Voltage and Heat Transfer Measurements Along an Arc-Plasma Wind-Tunnel Constrictor,” *Journal of Thermophysics and Heat Transfer*, Vol. 34, No. 3, 2020, pp. 626-639. <https://doi.org/10.2514/1.T5832>.
- [7] Ifergan, O., Berreby M., Mograbi, E. and Greenblatt, D., “Constricted arc plasma heated supersonic wind tunnel: model integral validation,” *Journal of Thermophysics and Heat Transfer*, Vol. 35, No. 4, 2021, pp. 888-893. <https://doi.org/10.2514/1.T6215>.
- [8] Gupta, R., Lee, K.-P., Thompson, R. A. and Yos, J. M., “Calculation and Curve Fits of Thermodynamic and Transport Properties for Equilibrium Air to 30000 K,” NASA RP-1260, 1991.
- [9] Anderson, J.D., “Modern compressible flow: with historical perspective,” 3<sup>rd</sup> Edition, McGraw-Hill, New York, 1990, Chapter 11.
- [10] Zucrow, M. J. and Hoffman. J. D. “Gas Dynamics,” Vol. 1, John Wiley & Sons, 1976.
- [11] Kidron, Y., Levy, Y., and Wasserman, M., “The EZAir CFD Solvers Suite: EZAir Theoretical and User’s Manual-Version 3.54,” ISCFDC TR 2016-19, Caesarea Industrial Park, Israel, Aug. 2016.

- [12] Menter, F.R., Kuntz, M. and Langtry, R., “Ten years of industrial experience with the SST turbulence model,” *Turbulence, Heat and Mass Transfer 4*, K. Hanjalić, Y. Nagano and M. Tummers (Eds), Begell House, Inc., 2003, pp. 625-632.
- [13] Wasserman, M., Mor-Yossef, Y., Shmueli, H., Loyevsky, A. and Mograbi, E., “Hybrid RANS/LES Simulation of Cavity-Stabilized Combustion in a Model Scramjet,” 60<sup>th</sup> Israeli Annual Conference on Aerospace Sciences, 2020, pp. 1-20.
- [14] Kirchberger, C., Wagner, R., Kau, H. P., Soller, S., Martin, P., Bouchez, M. and Bonzom, C., “Prediction and analysis of heat transfer in small rocket chambers,” AIAA Paper No. 2008-1260, 46th AIAA Aerospace Sciences Meeting and Exhibit, Reno, NV, 2008. <https://doi.org/10.2514/6.2008-1260>.
- [15] Takahashi, Y., Hisashi, K. and Abe, K., “The effects of radiative heat transfer in arc-heated nonequilibrium flow simulation,” *Journal of Physics D: Applied Physics*, Vol. 43, No. 18, 2010, 185201. <https://doi.org/10.1088/0022-3727/43/18/185201>.
- [16] Han, P. and Chen, X., “Modeling of the subsonic–supersonic flow and heat transfer in a DC arc plasma torch,” *Plasma Chemistry and Plasma Processing*, Vol. 21, 2001, pp. 249-264. <https://doi.org/10.1023/A:1007000431702>.
- [17] NASA, CEA., “NASA computer program for calculating of the Chemical Equilibrium with Applications,” NASA Glenn Research Center, Cleveland, OH, 2015. <https://www1.grc.nasa.gov/research-and-engineering/ceaweb/>
- [18] Bartz, D.R., “An approximate solution of compressible turbulent boundary layer development and convective heat transfer in convergent-divergent nozzles,” *ASME Journal of Fluid Engineering*, Vol. 77, No. 8, 1955, pp. 1235-1244. <https://doi.org/10.1115/1.4014652>.
- [19] Bartz, D.R., “A simple equation for rapid estimation of rocket nozzle convective heat transfer coefficients,” *Journal of Jet Propulsion*, Vol. 27, 1957, pp. 49-51. <https://cir.nii.ac.jp/crid/1570572700763427456>.
- [20] Smith, D.M., “A Comparison of experimental heat-transfer coefficients in a nozzle with analytical predictions from Bartz's methods for various combustion chamber pressures in a solid propellant rocket motor,” NASA-TM-X-61900, 1969.
- [21] Graham, R.W. and Boldman, D.R., “The Use of Energy Thickness in Prediction of Throat Heat Transfer in Rocket Nozzles,” NASA TN D-5356, 1969.
- [22] Kwong, K., Suchsland, K. and Tong, H., “Momentum/Energy Integral Technique (MEIT) User's Manual. No. ACUREX-UM-78-86 (7257),” ACUREX Corp/AEROTHERM, Mountain View, CAAEROSPACE Systems Div., 1978.

- [23] Dirker, J., and J.P. Meyer, "Convection heat transfer in concentric annuli," *Experimental Heat Transfer* Vol. 17, No. 1, 2004, pp. 19-29. University of Pretoria. <https://doi.org/10.1080/08916150490246528>.
- [24] Dunn, M.G. and Kang, S., "Theoretical and experimental studies of reentry plasmas," NASA-CR-2232, 1973.
- [25] D'Elia, C., "Development of Local Transient Heat Flux Measurements in an Axisymmetric Hybrid Rocket Nozzle," Master's Thesis, California Polytechnic State University, 2015, page 69. <https://doi.org/10.15368/theses.2015.4>.
- [26] Ruffin, A., "Numerical Investigation of Nozzle Thermochemical Behaviour in Hybrid Rocket Motors," PhD Thesis, Università Degli Studi Di Padova, 2015, page 31.
- [27] Pizzarelli, M., "Regenerative cooling of liquid rocket engine thrust chambers," Roma: Agenzia Spaziale Italiana, 2017. <https://doi.org/10.13140/RG.2.2.30668.92804>.
- [28] Thomas, B.G., Li, G., Moitra, A. and Habing, D., "Analysis of Thermal and Mechanical Behavior of Copper Molds during Continuous Casting of Steel Slabs," *Iron and Steelmaker*, Vol. 25, No. 10, pp. 125-143.
- [29] Jenkins, W.D., Digges, T.G., and Johnson, C.R., "Tensile properties of copper, nickel, and 70-percent-copper-30-percent-nickel and 30-percent-copper-70-percent-nickel alloys at high temperatures," *J. Res. Natl. Bureau Stds.*, Vol. 58, No. 4, 1957, pp. 201-211.
- [30] Srinath, L.S., "Advanced mechanics of solids," Tata McGraw-Hill, 2003, pages 274 and 316.
- [31] Pritchard, P.J. and Leylegian, J.C., "Fox and McDonald's Introduction to Fluid Mechanics," John Wiley & Sons, Inc., Danvers, MA, 8th Ed., 2011, pp. 357-362.
- [32] Haaland, S.E. "Simple and Explicit Formulas for the Friction Factor in Turbulent Flow," *Journal of Fluids Engineering*, Vol. 105, No. 1, 1983, pp. 89-90. <https://doi.org/10.1115/1.3240948>.
- [33] Idelchik, I.E. "Handbook of Hydraulic Resistance, (Revised and Augmented)," Hemisphere Publishing, 1986, Chapter 2.